# Postseismic fault creep on the Foothills thrust system following the 1989 Loma Prieta earthquake.

David D. Pollard, Roland Bürgmann and Paul Segall

**Final Technical Report**

Award # 1434-94-G-2447

to Stanford University
Department of Geological and Environmental Sciences
Stanford, CA 94305

Principal Investigator: David D. Pollard
(415) 723-4679 (phone)
(415) 725-0979 (FAX)
dpollard@pangea.stanford.edu

Program Element II. Evaluating earthquake potential

Research supported by the U.S. Geological Survey (USGS), Department of the Interior, under USGS award number 1434-94-G-2447. The views and conclusions contained in this document are those of the authors and should not be interpreted as necessarily representing the official policies, either expressed or implied, of the U.S. government.

FILE COPY

NON-TECHNICAL ABSTRACT

We use Global Positioning System (GPS) measurements to observe deformation at the Earth's surface following the 1989 M 7.1 Loma Prieta earthquake. The observed horizontal motions within a radius of ~20 km from the earthquake's epicenter differ significantly from those measured in the two decades preceding the earthquake. Our results indicate that anomalous shortening northeast of the San Andreas may be caused by slip along the Foothills thrust belt. These thrust faults may be capable of producing M6-7 earthquakes close to the densely populated Santa Clara valley. Continued postseismic deformation will eventually enhance, or retard future earthquakes on neighboring faults in the Bay Area.

# Postseismic fault creep on the Foothills thrust system following the 1989 Loma Prieta earthquake.

David D. Pollard[1], Roland Bürgmann[2,3] and Paul Segall[2]

[1] Department of Geological and Environmental Sciences, Stanford University, Stanford, CA

[2] Department of Geophysics, Stanford University, Stanford, CA

[3] now at Department of Geology, University of California, Davis, Davis, CA 95616

e-mail: burgmann@geology.ucdavis.edu, tel. 916-752-6808, FAX 916-752-6808

## INTRODUCTION AND MOTIVATION

Strain transients following large earthquakes may be responsible for clustering of seismic events in space and time. The postseismic velocity field in the epicentral region of the 1989 Loma Prieta earthquake differs significantly from displacement rates measured in the two decades preceding the event (Savage et al., 1994; Bürgmann et al., 1995). In 1994, we conducted a GPS survey of the Santa Cruz Mountains network that was last surveyed early in 1990. The new measurements allow us to resolve the spatial distribution of the postseismic displacements in detail. We find that the anomalous strain is best explained by aseismic oblique reverse slip on the sub-vertical San Andreas fault and reverse slip along a segment of the Foothills thrust belt at depths less than ~10 km. Rapid post-earthquake fault slip along the Foothills thrust belt located northeast of the San Andreas may be a precursory phenomenon to impending rupture, and could influence the timing of future earthquakes on nearby faults affected by the associated stress field.

*Postseismic Deformation*

Geodetic measurements subsequent to some large earthquakes show accelerated strain rates in the years to decades following the rupture (Thatcher, 1986). These observations may indicate a variation in deformation rates through the seismic cycle due to time-dependent deformation processes. For example, following the M 8.3 1906 San Francisco earthquake that ruptured the San Andreas fault over a length of up to 400 km (Lawson, 1908), strain rates in the Point Reyes and Point Arena triangulation networks north of San Francisco were about 2-3 times the rates measured in the 1970's (Thatcher, 1974). Other well documented examples of postseismic transients, not related to shallow afterslip, are from subduction-zone earthquakes in Japan (Kasahara, 1981; Thatcher, 1986).

Using simple models of postseismic relaxation, Thatcher (1974; 1983) concluded that existing deformation data can be explained by either the viscous relaxation of a ductile (asthenospheric) layer underlying an elastic (lithospheric) plate, or by the downward propagation of aseismic slip along a lower crustal extension of the fault zone. Many mechanical models of deep seated deformation transients following large dip-slip and strike-slip earthquakes have been proposed (Anderson, 1975; Bott and Dean, 1973; Budianski and Amazigo, 1976; Cohen, 1979; Lehner et

al., 1981; Li and Rice, 1987; Nur and Mavko, 1974; Rundle and Jackson, 1977; Savage and Prescott, 1978), however, there is a lack of adequate data to test and differentiate between them.

Fault creep at shallow depths (0 to 3 km) has been observed after several strike-slip earthquakes along the San Andreas fault system and typically decays exponentially within a few years of the earthquake (Bilham, 1989; Smith and Wyss, 1968). Postseismic creep at intermediate depth, on aseismic patches adjacent to seismic ruptures on the Calaveras fault, has been inferred from trilateration measurements (Oppenheimer et al., 1990). Openheimer et al. (1990) suggest that some main shocks along the Calaveras fault have been induced by postseismic slip from previous events that propagates toward the impending hypocentral area.

Observations of historic seismicity patterns indicate that earthquakes tend to propagate along fault zones rupturing fault segments immediately adjacent to, and within several years of a previously active break. Examples involving strike-slip faults have been reported along the North Anatolian fault system (Toksöz et al., 1979), in NE China preceding the 1975 Haicheng earthquake (Scholz, 1977), the Calaveras fault zone (Oppenheimer et al., 1990), and the San Andreas fault zone (Savage, 1971; Wood and Allen, 1973). In the 19th century, earthquakes along the San Andreas fault and the Hayward fault in the San Francisco Bay area occurred in clusters spread over several years (Ellsworth, 1990). This suggests the existence of transient processes that occur over characteristic time scales of several years. Lacking more geodetic data on the time-dependent deformation around previously ruptured fault segments, we can only speculate on the mechanics of postseismic deformation and the relation between strain transients and the clustering of earthquakes.

*The 1989 Loma Prieta earthquake and its aftermath*

The M 7.1 Loma Prieta earthquake of October 17, 1989, occurred on a previously unrecognized fault plane along a restraining bend of the San Andreas fault zone (Figure 1). The earthquake ruptured a buried 35-km long fault dipping 70° to the SW from about 8km to 18km depth, with comparable strike-slip and reverse dip-slip components of about 1.5 m, based on the distribution of aftershocks (Dietz and Ellsworth, 1990) and geodetic data (Lisowski et al., 1990a; Marshall et al., 1991; Snay et al., 1991; Williams et al., 1993). The slip distribution is more complex in detail, with slip of up to 5 m occurring on two patches to the NW and the SE of the hypocenter (Arnadottir and Segall, 1994; Beroza, 1991; Hartzell et al., 1991; Steidl et al., 1991; Wald et al., 1991).

Despite occurring away from the more densely populated regions of the San Francisco Bay area, damage from the Loma Prieta earthquake was considerable at distances of up to 100 km from the epicenter. Understandably, the earthquake has focused much attention on the possibility of earthquakes on faults even closer to major population centers. The Hayward fault last ruptured in 1836 and 1868 on its northern and southern segments, respectively, whereas the northern San Francisco Peninsula segment of the San Andreas fault slipped about 2-4 m during the 1906 earthquake and ruptured previously in 1838 (Ellsworth, 1990). In 1865, an earthquake in the southern San Francisco Bay area may have ruptured the San Andreas fault through the Santa Cruz Mountains, the Loma Prieta fault that ruptured in 1989, or possibly one of the faults of the Foothills thrust system NE of the San Andreas fault (Tuttle and Sykes, 1992). Several thrust faults along the San Andreas fault (Aydin and Page, 1984) may also represent significant seismic risks (Bürgmann, 1993; Bürgmann et al., 1994; Kovach and Beroza, 1993; Tuttle and Sykes, 1992).

Evidence that earthquakes on various fault strands in the San Francisco Bay area previously occurred in clusters or sequences, warrants intensive studies of the strain transients following the 1989 earthquake rupture. The Loma Prieta earthquake occurred in a geodetically well monitored region (Lisowski et al., 1991b), and offered the oportunity to determine post-earthquake strain anomalies with great precision and to better constrain models of postseismic deformation (Bürgmann et al., 1995; Savage et al., 1994).

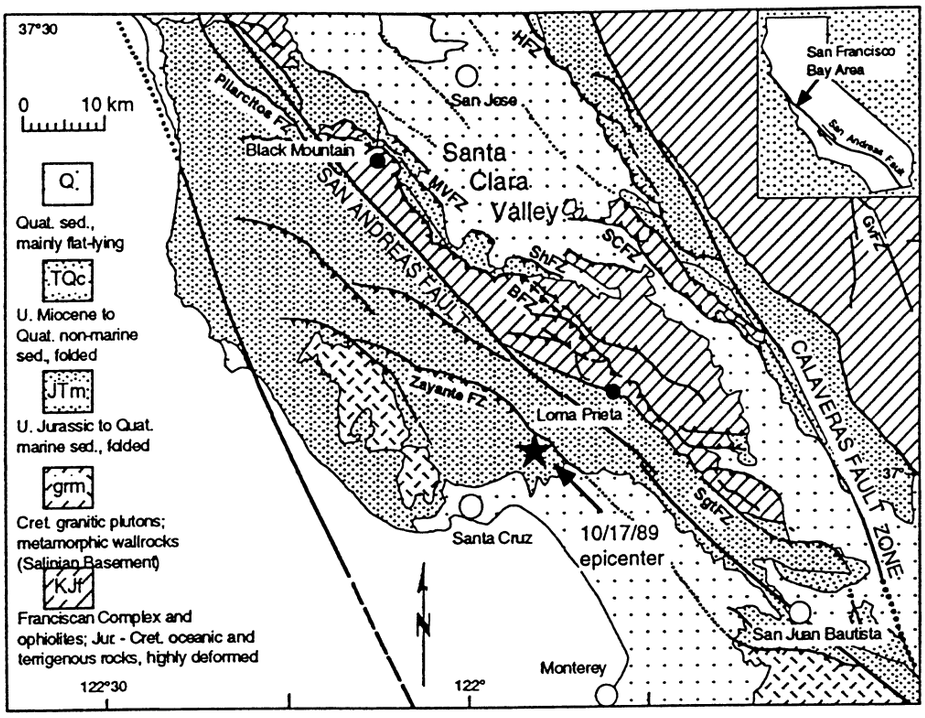


**Figure 1.** Location and Geologic map of the San Francisco Bay area showing major fault zones and localities described in text. Fault abbreviations: MVFZ, Monte Vista fault zone; ShFZ, Shannon fault zone; BFZ, Berrocal fault zone; SgtFZ, Sargent fault zone; SCrFZ, Silver Creek fault zone; EFZ, Evergreen fault zone. Modified from Bürgmann et al., 1994.

Measurements of surficial postseismic slip subsequent to the Loma Prieta earthquake find shallow displacements to be generally less than ~ 1 cm in the first year after the earthquake (Behr et al., 1990; Langbein, 1990; Rymer, 1990). Aftershocks occurred on the Loma Prieta rupture, as well as on adjacent faults, for years subsequent to the earthquake. However, the cumulative slip of aftershocks (~ 5 mm; (King et al., 1990) is too small to be detected geodetically. Behr et al. (1993) find that slip rates on the creeping section of the San Andreas fault near San Juan Bautista accelerated from a pre-earthquake rate of 7-8 mm/yr to a rate of ~13 mm/yr since the earthquake. About 2-3 cm of excess slip occurred over the northernmost 15 km of the creeping section in the 3 years following the earthquake, probably down to a depth of 1-3 km (Behr et al., 1993; Gwyther et al., 1992). Surficial creep rates on the southern Hayward fault have decreased from 3-9 mm/yr to about half the pre-earthquake rates. Near the fault's SE end, where the right-lateral creep rate was highest, it slipped left-laterally following the earthquake (Lienkaemper et al., 1992) with a possible reversal in early 1993 (Lienkarmper, 1993, pers. commun.). The magnitude of the

observed shallow creep transients (retardation as well as accelerations) is not expected to significantly affect the far-field displacement field of the southern San Francisco Bay area.

In this report we present Global Positioning System (GPS) data collected between October 1989 and May 1994 from an extensive geodetic network consisting of (1) the Black Mountain profile across the San Andreas fault 30 km NW of the Loma Prieta rupture (Bürgmann and Segall, 1991; Bürgmann et al., 1995); (2) the Loma Prieta profile through the epicentral region (Savage et al., 1994); (3) the 5-station Loma Prieta monitor network (Davis et al., 1989); and (4) the 22 station Santa Cruz Mountains network that was observed in March and April 1990 (Snay et al., 1991; Williams et al., 1993) and reoccupied in April and May 1994 with funding from the NEHRP program (Figure 2).

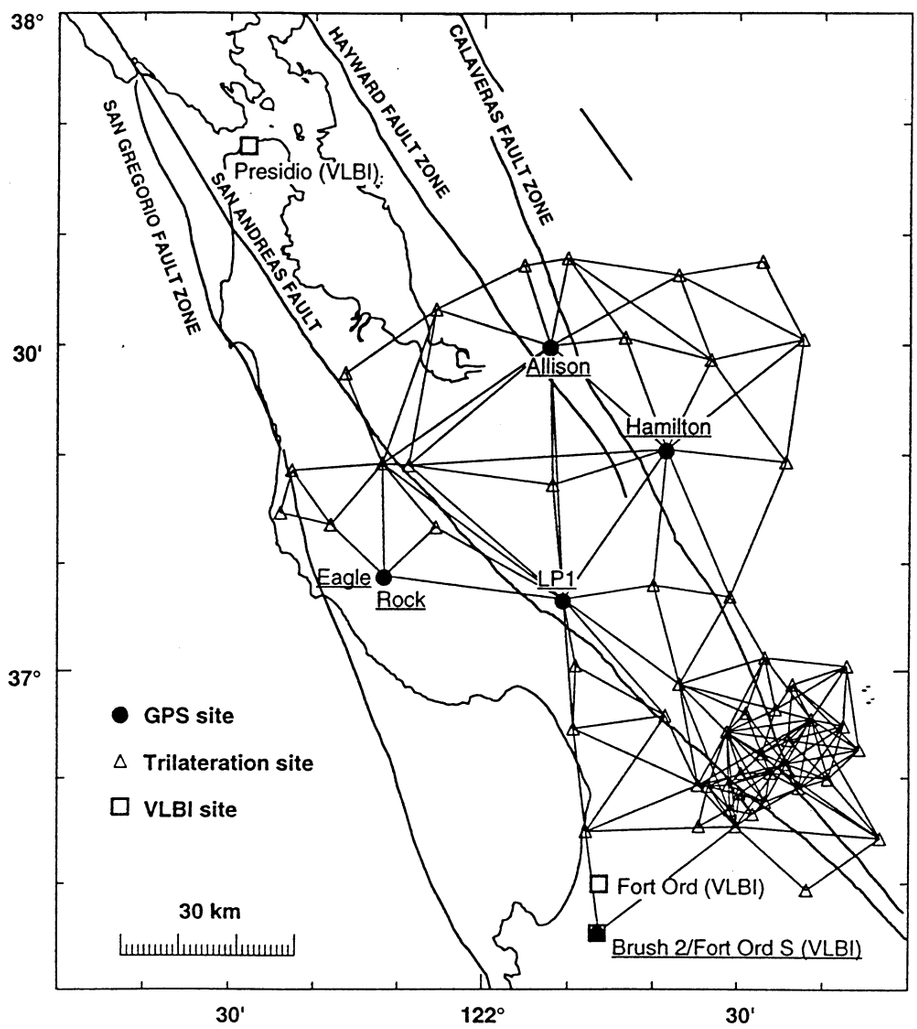


**Figure 2.** Pre-1989 Bay Area geodetic network consisting of geodolite trilateration network and GPS and VLBI stations in the south San Francisco Bay-Monterey Bay area.

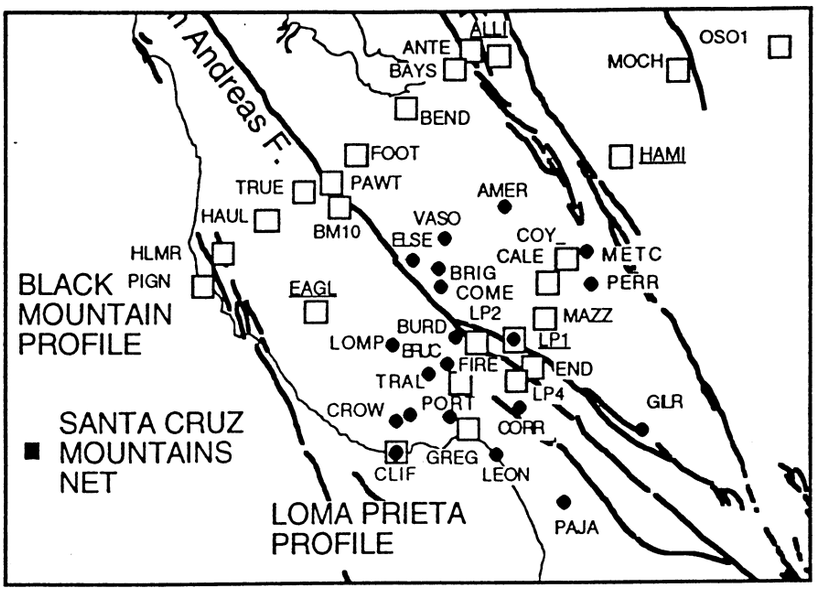


**Figure 2. cont.** (b) Post-1989 geodetic network used in this study consisting of two GPS profiles and Loma Prieta monitor network (underlined) across the SAF system (open squares), the VLBI stations at Ft. Ord and the Presidio (not shown), and the Santa Cruz Mountains network (filled circles).

The Loma Prieta monitor network had also been repeatedly surveyed with GPS for several years prior to the earthquake (Davis et al., 1989; Lisowski et al., 1990b). In addition to the GPS results, we also compute the displacements of Bay area VLBI stations relative to a North American reference frame (Clark et al., 1990). Ties of GPS sites to the collocated VLBI stations at Presidio, San Francisco and Ft. Ord near Monterey allow us to determine the local velocity field with respect to a remote reference frame. We also summarize results from leveling surveys across the epicentral region that provide details of the vertical postseismic displacements (Bürgmann, 1993). High precision vertical displacements are derived from a comparison of two occupations of a leveling line across the epicentral region of the Loma Prieta earthquake in March of 1990 (Marshall et al., 1991) and November of 1992 (Bürgmann et al., 1993). Our objectives are to determine the amount, nature, and source of deformation following the Loma Prieta earthquake and to examine the consequences for the potential of future earthquakes on the peninsular San Andreas fault and other faults in the San Francisco Bay region. In this report we focus on the results from the resurvey of the Santa Cruz Mountains network that was funded by the NEHRP program.

## GPS DATA COLLECTION, PROCESSING, AND ANALYSIS

Within the last 10 years the Global Positioning System (GPS) has proven to be a powerful and cost-effective tool for the measurement of relative displacement vectors in networks ranging from few hundred meters to thousands of kilometers in size (Davis et al., 1989; Dixon, 1991; Hager et al., 1991). Precision and accuracy of GPS are superior to triangulation and comparable to highest-quality trilateration measurements, with the added advantage of producing the full three-dimensional relative station displacements including the rotational component of deformation between two network occupations (Davis et al., 1989; Dixon, 1991; Hager et al., 1991). For networks of a scale of tens to thousands of km, GPS measurements nowadays achieve few-mm precision in the horizontal components and ~1 cm in the vertical. During the last 5 years, improvements of GPS receiver hardware, the constellation of the NAVSTAR GPS satellites, and the permanent tracking network and orbit improvements improved the precision of our measurements during this experiment.

*Data Collection*

Repeated surveys of the Black Mountain profile, the Loma Prieta profile, and the Bay area monitor network have been carried out since October 1989 (Figure 2; Bürgmann et al., 1995). Tie surveys between the two profiles allow us to connect the two subnetworks. In March and April of 1990 the U.S.G.S., the National Geodetic Survey, and Stanford University coordinated two weeks of observations of the profile and monitor networks and 22 additional sites, called here the *Santa Cruz Mountains network*, to measure the coseismic motions during the 1989 event (Snay et al., 1991; Williams et al., 1993). Table 1 summarizes the 1990 GPS campaign; the station names, occupation times, GPS receiver types used, and the agencies that collected the field data. In April and May of 1994 we reoccupied the Santa Cruz Mountains network concurrently with a USGS survey of the profile and monitor sites to better resolve the spatial distribution of the postseismic strain field (Bürgmann et al., 1994).

*Data Processing*

Our GPS data analysis principally follows the methods described by Davis and others (Davis et al., 1989). Doubly-differenced, ionosphere-free carrier phase observations are processed to estimate station coordinates, tropospheric zenith delays, and integer phase ambiguities. We use the Bernese GPS analysis software (Version 3.5; Beutler et al., 1987; Rothacher et al., 1990)) for parameter estimation. All double-difference carrier-phase residuals were visually inspected after processing the data with an automatic cycle-slip fixing program to remove remaining cycle slips and outliers.

The data were processed with a satellite elevation cut-off angle of 15°, because higher or lower cut-off angles appear to reduce the short-term repeatability of the station coordinates. We initially resolve 'wide-lane' (L5) ambiguities and fix the remaining linearly independent integer-cycle ambiguities using the ionosphere-free linear combination (L3). This combination of the two L-band frequencies (L1 & L2) eliminates most first-order effects of dispersive ionosphere delays that affect longer baselines. Baselines shorter than 3 km are not significantly affected by ionospheric variations, and are processed in the less noisy L1 frequency. Practically all integer-cycle ambiguities in the doubly differenced phase measurements were reduced to integer values in the local data. We did not attempt to resolve biases for baselines to or between tracking sites that are >

300-km long. Final coordinate estimates of the local stations were determined by processing the combined local and fiducial data and the resolved integer biases of the local data. In the same process, we estimate atmospheric propagation delay parameters (solving for a constant zenith delay parameter for each station for ~3-hour periods), satellite orbit parameters (through 1992), and synchronization errors (Davis et al., 1989).

Errors in the orbit information broadcast by the GPS satellites can be significantly reduced by monitoring the satellites from global tracking networks with well known station coordinates (Larson et al., 1991). We improve GPS satellite orbits utilizing data from fiducial tracking stations operated by the U.S. National Geodetic Survey (NGS) in Mojave, California, Westford, Massachusetts, and Richmond, Florida, that are constrained to their well known coordinates (ITRF-92 station coordinates and velocities). During the June 1991 campaign we added data from tracking stations at Penticton and Yellowknive in Canada, and from Kokee on Hawaii to compensate for the lack of data from the three fiducial stations we commonly used. For data collected since January 1993 we utilize precise IGS (International Geodetic Survey) orbits derived from the orbits computed by all IGS data centers and tie our local stations only to the nearest IGS tracking sites in California (Quincy and Goldstone).

*Data Precision And Accuracy*

The short-term precision of GPS measurements depends on error sources related to satellite and receiver clocks, propagation delays, satellite orbit and constellation characteristics, length and time of observation, the geographic location of a network, receiver types and post-processing software, and set-up procedures (Larson and Agnew, 1991). Average day-to-day repeatabilities are about 3 mm in the horizontal components and about 1 cm in the vertical. We note apparent improvements in day-to-day repeatabilities from >10-hour observation times and in more recent surveys that benefitted from better satellite coverage, receiver hardware, and the use of precise IGS orbits.

| GPS WEEK | 531 | | | | | | 532 | | | | | | | 533 | | | | | | | | 534 | | | | | | 535 | | | | |
|---|---|---|---|---|---|---|---|---|---|---|---|---|---|---|---|---|---|---|---|---|---|---|---|---|---|---|---|---|---|---|---|---|
| SUBNETWORK / DATE | 3/12 | 3/13 | 3/14 | 3/15 | 3/16 | 3/17 | 3/18 | 3/19 | 3/20 | 3/21 | 3/22 | 3/23 | 3/24 | | | 3/27 | 3/28 | 3/29 | 3/30 | 3/31 | | 4/2 | 4/3 | 4/4 | 4/5 | 4/6 | | | | | | 4/11 |
| STATIONS / DAY | 71 | 72 | 73 | 74 | 75 | 76 | 77 | 78 | 79 | 80 | 81 | 82 | 83 | 84 | 85 | 86 | 87 | 88 | 89 | 90 | 91 | 92 | 93 | 94 | 95 | 96 | 97 | 98 | 99 | 100 | | 101 |
| NGS (TI4100) | | | | | | | | | | | | | | | | | | | | | | | • | • | | | | | | | | |
| MOUNT TAMALPAIS 2 | | | | | | | | | | | | | | | | | | | | | | | • | • | | | | | | | | |
| DIABLO ECC RM 2 1962 | | | | | | | | | | | | | | | | | | | | | | | • | • | | | | | | | | |
| MOCHO | | | | | | | | | | | | | | | | | | | • | • | | | • | • | | | | | | | | |
| LOMA PRIETA CGS | | | | | | | | | | | | | | | | | | • | • | | | | | | • | | | | | | | |
| CHAMBERLAIN | | | | | | | | | | | | | | | | | | • | | • | | | | | • | • | | | | | | |
| PERRYS | | | | | | | | | | | | | | | | | • | • | | | | | | | • | • | | | | | | |
| METCALF | | | | | | | | | | | | | | | | | • | • | | | | | | | • | | | | | | | |
| GILROY | | | | | | | | | | | | | | | | • | • | | | | | | | | | | | | | | | |
| AMERICAN | | | | | | | | | | | | | | | | • | • | | | | | | | | | • | | | | | | |
| VASONA | | | | | | | | | | | | | • | | | • | | | | | | | | | | | | | | | | |
| EL SERENO | | | | | | | | | | | | | • | | | • | | | | • | | | | | | | | | | | | |
| ODAMA | | | | | | | | | | | | | • | | | • | | | | | | | | | | | | | | | | |
| ST JOSEPHS | | | | | | | | | | | | • | • | | | | | | | | | | | | | | | | | | | |
| BRIGGS | | | | | | | | | | | | • | | | | | | | | • | | | | | | | | | | | | |
| COMEX | | | | | | | | | | • | • | | | | | | | | | | | | | | | | | | | | | • |
| BRUCE | | | | | | | | | | | • | • | | | | | | | | | | | | | | | | | | | | |
| LOMPICO | | | | | | | | | | | • | • | | | | | | | | | | | | | | | | | | | | |
| BURDETT | | | | | | | | | | • | • | | | | | | | | | | | | | | | | | | | | | • |
| TRAILL | | | | | | | | | • | | | | | | | | | | • | | | | | | | | | | | | | • |
| PAJARO 3 | | | | | | | | | • | • | | | | | | | | | | | | | | | | | | | | | | • |
| CROWELL RM 3 | | | | | | | | | • | • | | | | | | | | | | | | | | | | | | | | | | • |
| SANTA CRUZ AZIMUTH | | | | | | | | | • | | | | | | | | | | • | | | | | | | | | | | | | |
| CORRALITOS | | | | | | | | | • | • | • | • | • | | | • | • | • | • | • | | | • | • | • | | | | | | | • |
| NASA GSFC 7241 | | | | | | | | | | | | | | | | | | | | | | | | | | | | | | | | |
| STANFORD (Trimble) | | | | | | | | | | | | | | | | | | | | | | | | | | | | | | | | |
| Porter | | | | | | | | | | | | | | | | | • | • | • | | | | | | | | | | | | | |
| Leon | | | | | | | | | | | | | | | | | • | | | | | | | | | | | | | | | |
| Pajaro 3 | | | | | | | | | | | | | | | | | • | | | | | | | | | | | | | | | |
| R121 | | | | | | | | | | | | | | | | | | • | • | | | | | | | | | | | | | |
| Crowell | | | | | | | | | | | | | | | | | | • | | | | | | | | | | | | | | |
| R57 | | | | | | | | | | | | | | | | | | • | • | | | | | | | | | | | | | |
| Traill | | | | | | | | | | | | | | | | | | | • | | | | | | | | | | | | | |
| Cliff | | | | | | | | | | | | | | | | | | | | | | | | | | | | | | | | |
| U.S.G.S. (TI4100) | | | | | | | | | | | | | | | | | | | | | | | | | | | | | | | | |
| PIGN | | | | | | • | | | | | | | | | | | | | | | | | • | | • | | | | | | | |
| HLMR | | | | | | | | | | | | | | | | | | | | | | | • | | | | | | | | | |
| HAUL | | | | | | | | | | | | | | | | | | | | | | | | | • | | | | | | | |
| TRUE | | | | | | | | | | | | | | | | | | | | | | | | • | • | | | | | | | |
| BM10 | | | | | | | | | | | | | | | | | | | | | | | | • | | | | | | | | |
| PAWT | | | | | | | | | | | | | | | | | | | | | | | | | • | | | | | | | |
| FOOT | | | | | | • | | | | | | | | | | | | | | | | | | • | • | | | | | | | |
| BEND | | | | | | | | | | | | | | | | | | | | | | | | • | | | | | | | | |
| BAYS | | | | | | | | | | | | | | | | | | | | | | | | • | | | | | | | | |
| ANTE | | | | | | | | | | | | | | | | | | | | | | | • | | | | | | | | | |
| brush 2 1978 | | | | | | | | | | | | | | | | | | | | | | | • | | | | | | | | | |
| luces pt | | | | | | | | | • | | | | | | | | | | | | | | | | | | | | | | | |
| CLIFF | | | | | | | | | • | | | | | | | | | | | | | | | | | | | | | | | |
| GREGOR | | | | | | | | | • | | | | | | | | | | | | | | | | | | | | | | | |
| FIRE | | | | | | | | | • | | | | | | | | | | | | | | | | | | | | | | | |
| LP4 | | | | | | | | | | • | | | | | | | | | | | | | | | | | | | | | | |
| LP2 | | | | | | | | | | • | | | | | | | | | | | | | | | | | | | | | | |
| END | | | | | | | | | • | • | • | | | | | | | | • | | | | | | | | | | | | | |
| LP1 | | | | | | | | | | • | | | | | | | | | | | | | | | | | | | | | | |
| CALERO | | | | | | | | | | • | | | | | | | | | | | | | | | | | | | | | | |
| MAZZONE | | | | | | | | | | | • | | | | | | | | | | | | | | | | | | | | | |
| COY | | | | | | | | | | | • | | | | | | | | | | | | | | | | | | | | | |
| OSO RM1 | | | | | | | | | | | • | | | | | | | | | | | | | | | | | | | | | |
| MOCHO | | | | | | | | | | | | | | | | | | | • | | | | | | | | | | | | | |
| ALLISON | | | | | | | | | | | | | | | | | | | • | | | | | | | | | | | | | |
| EAGLE | | | | | | | | | | | • | | | | | | | | • | | | | | | | | | | | | | |
| HAMILTON | | | | | | | | | | | | | | | | | | | • | | | | | | | | | | | | | |
| LOMA NCER | | | | | | | | | | | | | | | | | | | | | | | | | | | | | | | | |
| CORD | | • | • | • | • | | | | | | | | | | | | | | | | | | | | | | | | | | | |
| JACK | | | | | • | • | | | | | | | | | | | | | | | | | | | | | | | | | | |
| SWEE | | | | | • | • | | | | | | | | | | | | | | | | | | | | | | | | | | |
| WHAL | | | | | • | • | | | | | | | | | | | | | | | | | | | | | | | | | | |
| Pt. Reyes NCMN | | • | | | | | | | | | | | | | | | | | | | | | | | | | | | | | | |
| Pt. Reyes HD | | • | | • | | | | | | | | | | | | | | | | | | | | | | | | | | | | |
| Pt. Reyes Hill | | • | | | | | | | | | | | | | | | | | | | | | | | | | | | | | | |
| STANFORD (Trimble) | | | | | | | | | | | | | | | | | | | | | | | | | | | | | | | | |
| PIGN | | | | | | | | | | | | | | | | | | | | | | | | • | | | | | | | | |
| HLMR | | | | | | | | | | | | | | | | | | | | | | | | • | | | | | | | | |
| HAUL | | | | | | | | | | | | | | | | | | | | | | | | • | | | | | | | | • |
| TRUE | | | | | | | | | | | | | | | | | | | | | | | • | | | | | | | | | • |
| BM10 | | | | | | | | | | | | | | | | | | | | | | | • | | | | | | | | | • |
| PAWT | | | | | | | | | | | | | | | | | | | | | | | • | | | | | | | | | • |
| FOOT | | | | | | | | | | | | | | | | | | | | | | • | • | • | | | | | | | | • |
| BEND | | | | | | | | | | | | | | | | | | | | | | • | | | | | | | | | | • |
| BAYS | | | | | | | | | | | | | | | | | | | | | | • | | | | | | | | | | • |
| ANTE | | | | | | | | | | | | | | | | | | | | | | • | | | | | | | | | | • |
| TOTAL OCCUPATIONS | 0 | 4 | 1 | 2 | 4 | 5 | 0 | 0 | 10 | 10 | 10 | 5 | 5 | 0 | 0 | 5 | 9 | 9 | 14 | 5 | 0 | 4 | 13 | 14 | 10 | 3 | 0 | 0 | 0 | 0 | | 5 |

**Table 1.** Occupation schedule of the 1990 survey of the complete south Bay Area GPS network coordinated by Stanford, the USGS, and the NGS crustal deformation groups.

## PRE-LOMA PRIETA EARTHQUAKE DISPLACEMENT FIELD

Trilateration measurements have been carried out throughout the San Francisco Bay area during the two decades before the Loma Prieta earthquake (Lisowski et al., 1991b). Except for the effects of the 1979 Coyote Lake and the 1984 Morgan Hill earthquakes the velocity field appears to have been constant over that time period. Figure 3 shows the horizontal velocity field in the region based on (1) 20 years of trilateration data, (2) several years of GPS data for the Loma Prieta monitor stations, and (3) Very Long Baseline Interferometry (VLBI) data collected at Presidio (6 years), Fort Ord (5 years) and Fort Ord S (1 year). The VLBI station velocities are shown relative to a North American reference frame defined by a fixed origin at the Westford, Massachusetts VLBI station and a fixed azimuth from Westford to the VLBI station at Richmond, Florida (Clark et al., 1990). All other velocities were computed by applying the VLBI velocity of Fort Ord to Brush 2, co-located with Fort Ord S, 8.9 km to the south. The velocity of the easternmost stations of the trilateration network are small, indicating that most of the deformation zone between the Pacific and North American plates is contained within the network. The trilateration network, that by itself offers no constraint on rigid-body network rotations or translations, is also linked to the GPS network through common benchmarks (or ties between co-located trilateration and GPS benchmarks) at Loma Prieta, Eagle Rock, Allison, Hamilton, and Brush 2 (Figure 2).

The velocity field in the southern San Francisco Bay area accommodates 38 ± 5 mm/yr of right-lateral plate-boundary shear across a width of about 120 km, as described by Lisowski et al. (1991b). The velocity vectors are approximately parallel to the regional trend of the San Andreas fault system and do not appear to be influenced by the local left bend in the San Andreas fault trace through the Santa Cruz Mountains. The displacement field broadens towards the northwest. Whereas the (creeping) segment of the San Andreas fault southeast of San Juan Bautista accomodates most of the plate motion (~ 35 mm/yr), slip becomes distributed between the San Andreas, Hayward, and Calaveras faults in the San Francisco Bay area.

Deviations from the simple shear flow pattern are apparent along the southern Calaveras fault in the closely spaced Hollister network. Stations just east of the Calaveras fault appear to move towards the fault at an oblique angle. It is possible that the complex series of creeping and locked fault segments along the Calaveras fault (Oppenheimer et al., 1990) causes the more complicated displacement rate vectors. Alternatively the southern Calaveras and or the southern Sargent faults may accommodate convergence by oblique slip (Matsu'ura et al., 1986).

Only few of the postseismic GPS benchmarks have been surveyed before the Loma Prieta earthquake, so that in order to compare pre- and post-earthquake velocities we must interpolate between stations. To do this, we developed a mechanical model of the preseismic displacement field (Figure 3b). Uniform-slip boundary elements in an elastic, homogenous, and isotropic half space represent the Bay area faults. Inter-seismic shear about a locked upper crustal strike-slip fault can be approximated by slip on a buried fault plane below the seismic zone at a rate comparable to the average geologic slip rate of the fault (e.g. (Lisowski et al., 1991b). Surface creep on the Hayward, Calaveras, and the central San Andreas fault can be modeled by shallow fault elements. Our objective here is not to find a correct physical model of Bay area tectonics, but to develop a close fitting approximation of the preseismic velocity field which can be used to compute the expected velocities of stations for which preseismic velocities are not available.

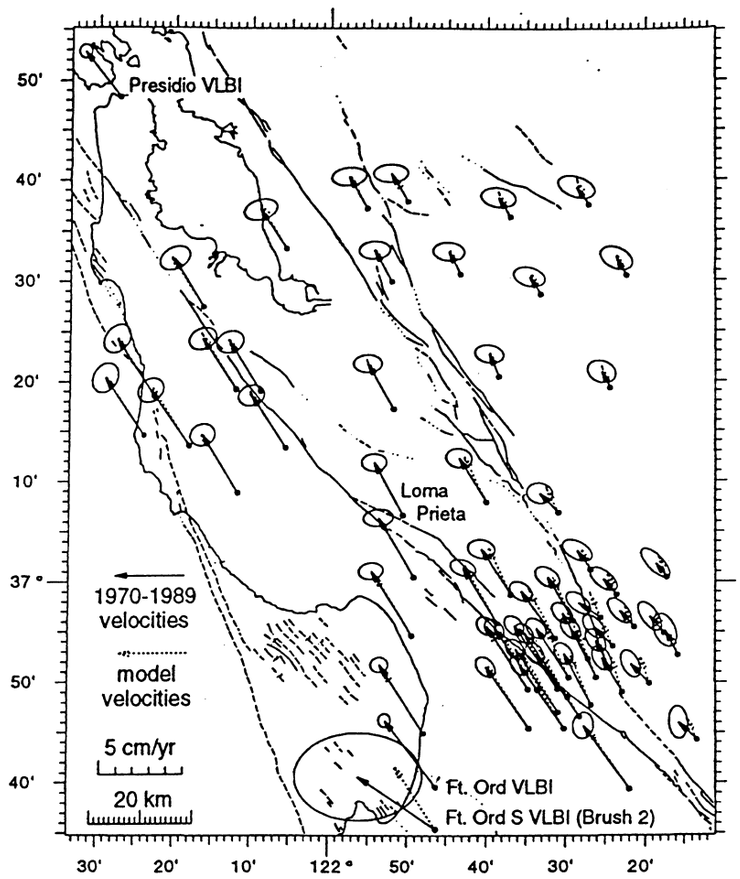


**Figure 3.** (a) Pre-Loma Prieta earthquake site velocities (solid arrows with 95% error ellipses) in the southern San Francisco Bay region determined from VLBI, trilateration, and GPS measurements. The VLBI velocity of Fort Ord is applied to the GPS and trilateration site Brush 2 to the south. All displacements are shown relative to the North American reference frame. Dashed arrows show displacement vectors computed from a mechanical model of the preseismic deformation (Fig. 3b) used to compute velocities at the postseismic network stations.

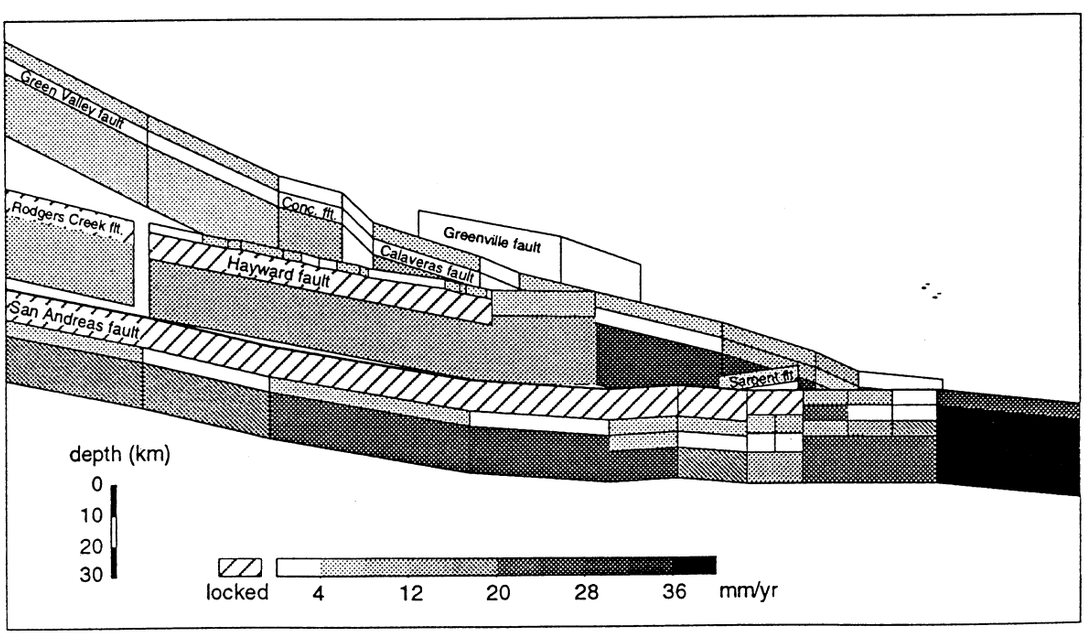


**Figure 3. cont.** (b) Slip rates on segments of the Bay area fault system used to model the preseismic displacement field. The fault elements that end at 30 km depth in the plot continue to 1000 km depth in the model.

We develop a best fitting model using a linear inversion method (Du et al., 1992) that inverts the horizontal displacement field (trilateration and GPS data) for right-lateral strike slip magnitudes on individual segments of the Bay area faults shown in Figure 3b. All faults are assumed to be vertical with no dip-slip component. A priori constraints of the starting model come from geologically determined slip rates (closely based on a compilation of Lienkamper et al. (1992)). The fault model predicts the following features: (1) Deep (> 15 km) slip on the peninsular segment of the San Andreas fault at about 20-25 mm/yr; (2) deep slip (> 11 km) on the Hayward fault at about 14 mm/yr; (3) deep slip (> 10 km) on the northern Calaveras fault at about 10-12 mm/yr and at up to 28 mm/yr on the southern Calaveras fault; and (4) shallow creep on the East Bay and southern San Andreas at rates comparable to the measured a priori values. The deep slip rate on the southern Calaveras fault appears too high and may be related to the effects of the Coyote Lake and Morgan Hill earthquakes that occurred on the fault during the measurement period.

Figure 3a shows a comparison of the measured station velocities and the model displacements with the station at Loma Prieta serving as reference site (i.e., the model velocities are adjusted so that Loma Prieta moves at the measured velocity in the North American reference frame). We note that most velocities are fit well within their 95% uncertainties except for several of the sites near the southern Calaveras fault. The model slightly underpredicts the velocities southwest of the San Andreas fault south of Loma Prieta. The model faults shown in Figure 3b can now be used to compute the predicted preseismic displacements of the postseismic network (Figure 4). Differences between the observed post-1989 displacements and this model describe the postseismic strain anomaly.

## POST-LOMA PRIETA EARTHQUAKE DISPLACEMENT FIELD

*Horizontal displacements from GPS*

Figure 4 shows the velocity field of repeatedly surveyed GPS and VLBI stations following the 1989 Loma Prieta earthquake assuming linear displacement rates. The velocities of the VLBI stations Fort Ord S and Presidio are shown relative to a North American reference frame defined by a fixed origin at the Westford, Massachusetts VLBI station and a fixed azimuth from Westford to the VLBI station at Richmond, Florida (Clark, et al., 1990). The GPS network is tied to the VLBI reference frame through the common site at Fort Ord S/Brush 2.

We assume constant displacement rates in our determination of the site velocities. The GPS station velocities were determined using a least squares algorithm (coded by M. Murray) that computes station velocities relative to a local reference station and the associated 95% error ellipses from the station coordinates and the associated covariance matrices of each campaign. However, the time series along the Loma Prieta profile suggest a decay in the postseismic displacement rates (Savage et al., 1994; Bürgmann et al., 1995). Savage et al. (1994) found that postseismic decay was particularly evident in the SAF-normal component. We see no evidence of rate variations along the Black Mountain profile. We will develop new tools to determine time-dependent deformation rates from our repeatedly surveyed station coordinates. Furthermore, we note that stations MAZZ, CALE, COY_, and HAMI all show significant convergence towards Loma Prieta. The estimates of the vertical displacement component did not show a trend above the data noise.

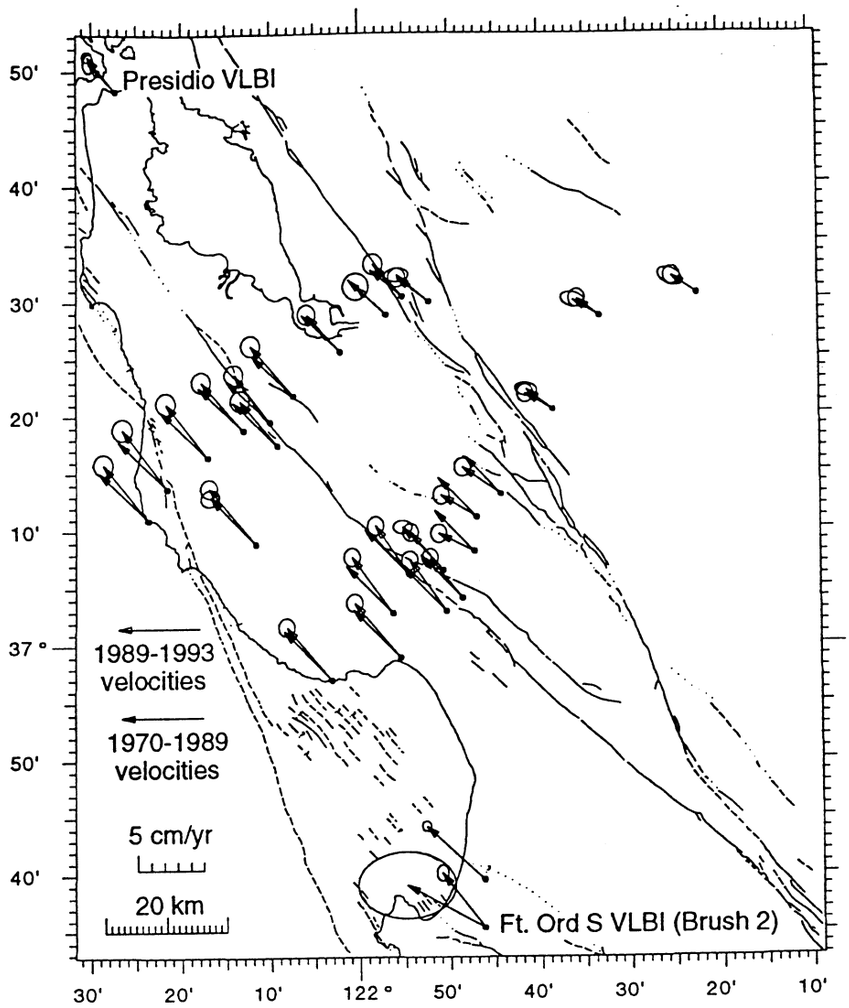


**Figure 4.** Postseismic velocity field from GPS and VLBI measurements. The velocities and associated 95% error ellipses were computed relative to stable North America. The GPS network is tied to the VLBI reference frame through the common site at Fort Ord S-Brush 2.
Vectors with filled arrowheads show the measured pre-seismic velocities (with error ellipses) or displacement rates computed from a mechanical model. The pre-earthquake velocities are shown under the assumption that Mt. Oso was not affected by the postseismic transients.

A resurvey of the Santa Cruz Mountains network in the Spring of 1994 allows us to compute the total postseismic displacements of all sites since early 1990. Figure 5 shows the total displacements for all sites between March/April of 1990 and April/May of 1994. The stations of the Santa Cruz Mountains network added considerable spatial resolution of the postseismic displacement field. Overall, the sites confirm the existence of considerable contraction across the western Santa Clara Valley. This zone is associated with local left-lateral shear northwest of the SAF. We find that the zone of anomalous contraction reaches at least half way between the Loma Prieta and Black Mountain profiles (i.e., there is notable contraction between stations VASO and AMER). Stations located to the southwest of the SAF indicate fault parallel, right-lateral shear.

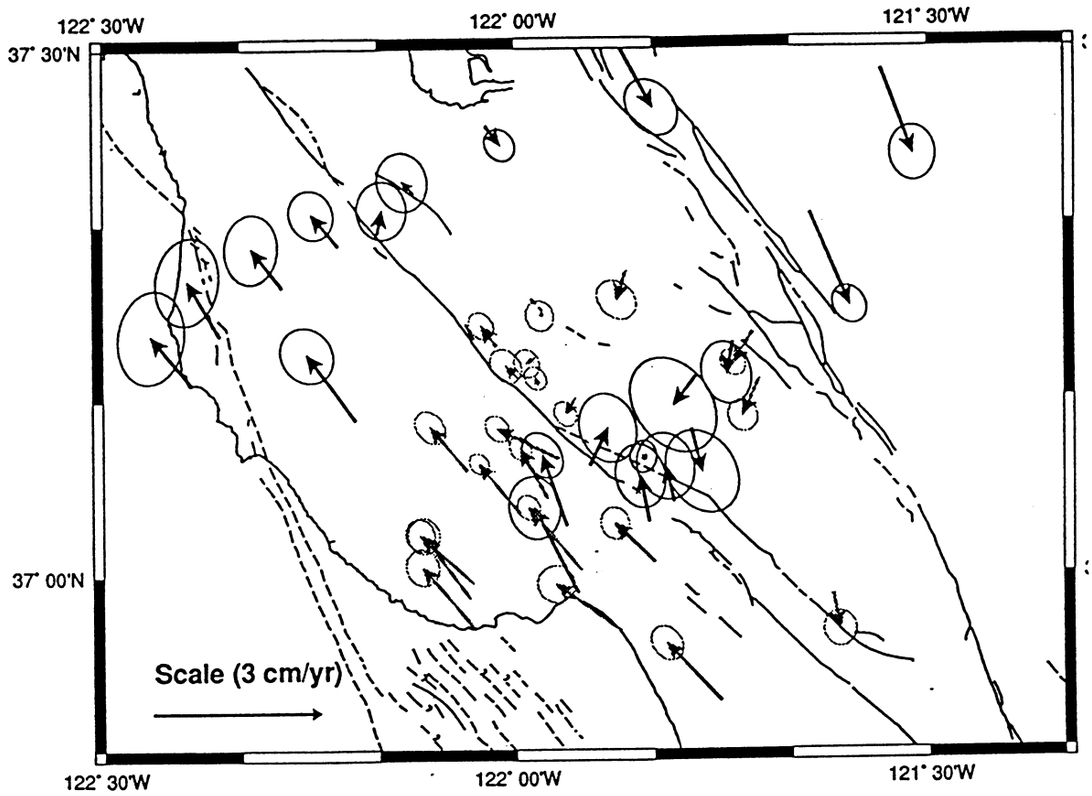


**Figure 5.** Postseismic displacements relative to Loma Prieta of stations within about 60 km of the 1989 epicenter between April 1990 and April 1994. Note the zone of localized contraction northwest of Loma Prieta that is superimposed over the regional right-lateral distributed shear. These data are being used in the following analysis of the postseismic anomaly. Grey-shaded vectors are from stations of the Santa Cruz Mountains network.

*Vertical displacements from leveling*

The observed elevation changes are shown in Figure 6 together with a schematic cross-section of active fault zones along the line (based on McLaughlin, 1990) and the distribution of two years of Loma Prieta aftershocks starting 30 days after the earthquake. Northeast of the San Andreas fault we find a series of reverse structures dipping towards the SW. The aftershocks outline the dipping Loma Prieta rupture below 10 km, a vertical San Andreas fault above 10 km, and rather distributed seismicity NE of the San Andreas fault.

Assuming zero elevation change at Capitola, an elevation rise of about 2 cm occurs about 15 km to the northeast, whereas the last 15 km of the line subsided by up to 3.5 cm. Notable features of the uplift pattern are a broad (apparently with two maxima) uplift zone between 10 km and just east of Loma Prieta and the large down drop that appears to extend past the northeastern end of the line. We note that the steepest displacement gradient occurs directly in the hanging wall of the Berrocal fault zone. The uplift exceeds by about an order of magnitude the average late Cenozoic uplift rate of the range (Bürgmann et al., 1994).

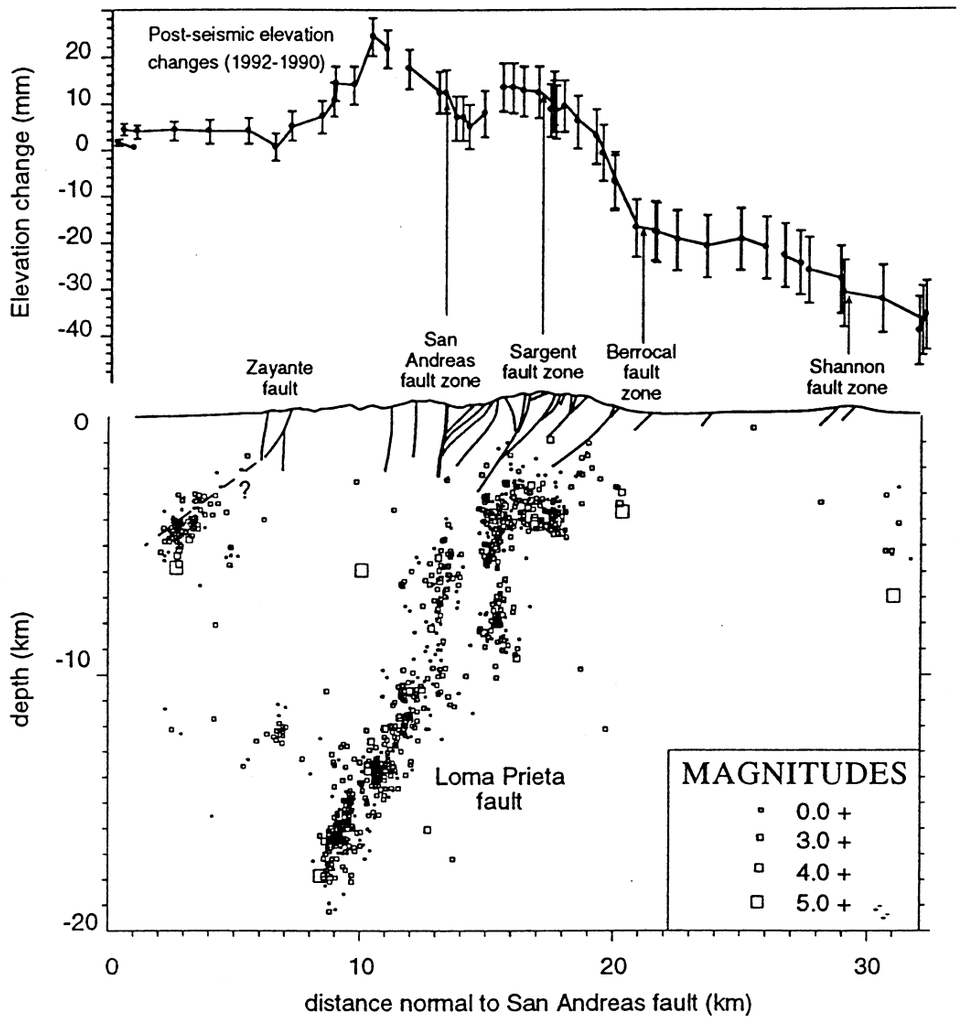


**Figure 6.** SW-to-NE cross-section (Gregor to Coy in Figure 2b) of the geology (modified from McLaughlin (1990)) and Loma Prieta aftershocks across the San Andreas fault system. Also shown are the postseismic elevation changes from leveling (Bürgmann, 1993). Note that the steepest gradient in the elevation changes is located in the hanging wall of the Berrocal fault, which also appears to be associated with high aftershock activity. The plotted earthquakes are from a 15 km wide zone centered on the line of section and include all well-located events from one month after the Loma Prieta earthquake until December, 1992.

## DATA INTERPRETATION AND MODEL

*Postseismic strain anomaly*

Over the-60 km long Black Mountain profile, from the Pacific coast (Pigeon Pt.) to just east of the Hayward fault (Antelynx), 22 ± 5 mm/yr of right-lateral shear has occurred along the profile since the earthquake. The postseismic displacement rates do not differ significantly from the pre-earthquake rate of 20 ± 4 mm over approximately the same width. Whereas only minor changes have been observed along the Black Mountain profile 44 km northwest of the 1989 epicenter, measurements of the Loma Prieta profile show significant changes in displacement rates from pre-earthquake values (Lisowski et al., 1991a). GPS stations within 20 km from the San Andreas fault, show significant deviations in both magnitude and orientation from preseismic values. The difference between the post- and pre-earthquake velocities shown in Figure 7 represents the component of the measured signal (the comparison of the April 1990 and 1994 measurements) that exceeds the secular deformation field. At sites where velocities have been measured before and after the earthquake the difference between the two vectors and its uncertainty is shown. Elsewhere, the predicted postseismic displacements from the boundary element model are subtracted from the postseismic measurements, and the error ellipses are determined under the assumption that the errors in the pre-earthquake velocities are equal to those in the post-earthquake data. The plotted velocity vectors are shown relative to the motion of the station LP1_ on Loma Prieta. Not that the velocities of sites along the Black Mountain profile, stations along the coast, and stations northeast of the Calaveras fault all show a northwest-ward motion of a few mm. This suggests that in an external reference frame with no anomalous motion at great distances from the epicenter the site at Loma Prieta moved a few millimeters to the southeast.

Significant velocity increases and reorientations occurred in the near field of the earthquake rupture. Fault-parallel right-lateral velocities increased to the southwest of the San Andreas. To the northeast of Loma Prieta we see evidence for a local zone of *left-lateral* shear, all sites in the eastern Santa Clara Valley move westerly relative to Loma Prieta and stations to the northwest of Loma Prieta. There has also been a large fault-normal contraction centered to the northeast of the San Andreas fault. We find that the postseismic displacement rates at distances >~20 km from the epicenter are indistinguishable, within errors, from secular displacement rates. The uplift pattern determined from leveling (Figure 6) is considered to be caused by transient deformation only. Geologic uplift rates (Bürgmann et al., 1994) and uplift rates from our model of the preseismic deformation field are ≤1 mm/yr, one order of magnitude less than the measured uplift.

*Models of post-Loma Prieta deformation*

The postseismic displacement pattern following the Loma Prieta earthquake has also been interpreted by Linker and Rice (1991) and by Lisowski and others (1991a) and Savage and others (1994). Linker and Rice (1991; 1995) model the displacement field resulting from the interaction of the earthquake rupture with a linear viscoelastic relaxation zone below, that represents the deep aseismic portion of the fault. They also developed a non-linear model that assumes rate- and state-dependent friction on the deep aseismic region of the fault zone. Their models, involving a relatively deep deformation source below the coseismic rupture, predict the fault-parallel velocities of the Loma Prieta profile well, but do not predict the observed fault-normal velocity component and appear to overpredict the rates in the Black Mountain profile.

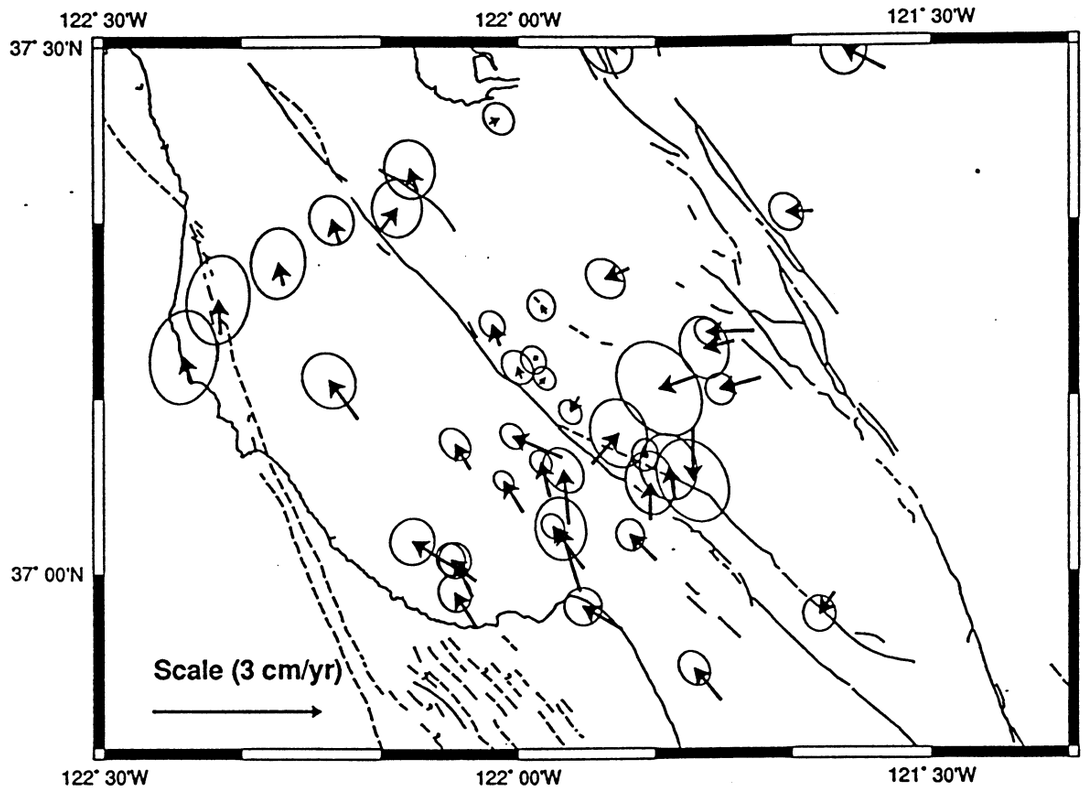


**Figure 7.** Postseismic station velocities with preseismic displacement rates subtracted from measured rates. The velocities reflect the average rate between April 1990 and April 1994 and only include surveys at those two epochs. The residual vectors are shown relative to Loma Prieta. The consistent northwestward motion of distant sites suggest that Loma Prieta itself moved southeastward in an external reference frame (Fig. 8).

The model proposed by Savage and others (Lisowski et al., 1991a; 1994) involves strike-slip shear on the Loma Prieta rupture plane (0.83 m/yr at 4 to 11 km depth), and fault-normal collapse of the fault zone at a rate of 0.11 m/yr (3 to 7 km depth) to explain the anomalous site-velocity vectors along the Loma Prieta profile. In addition to the postseismic deformation sources Savage and others (1994) also estimate right-lateral slip on vertical dislocations below the San Andreas and Calaveras faults that represent the background displacement field. That is, instead of subtracting the preseismic displacement field from the postseismic measurements, they solve for the postseismic anomaly *and* the secular displacement rates. This model successfully predict the horizontal displacement measurements.

Previously, we proposed a model involving postseismic creep on two faults that reproduces the GPS results based on two years of data (Bürgmann and Segall, 1991). Aseismic strike slip at a rate of 0.17 m/yr on the Loma Prieta rupture and reverse slip at a rate of 0.10 m/yr on a thrust fault of the Sargent-Berrocal fault zone can explain the observed horizontal motions until August 1991. Because the slip patch on the Berrocal fault was as shallow as 1 km, the model predicts a very large vertical signal. However, we find that the observed uplift (Figure 6) suggests that either slip was significantly less, or deeper, than inferred from the early GPS-derived results. We will first discuss the different types of previously suggested models, and then go on to present our preferred model.

*Mechanical models from nonlinear inversions*

We model the displacements with rectangular dislocations in an elastic half-space (Okada, 1985). The nonlinear optimization algorithm NPSOL determines fault parameters (length, depth, width, dip, strike, location, and the amounts of strike slip, dip slip, and opening) of one or two faults that best reproduce the GPS and leveling data by minimizing the weighted residual sum of squares (Arnadottir and Segall, 1994; Williams et al., 1993). We developed a series of models to evaluate the previously proposed models of postseismic relaxation and to develop a model that best satisfies geologic and geophysical constraints (Table 2). The quality of fit of these models is derived from the GPS data set shown in Figure 4, that is, it does not include the Santa Cruz Mountains network stations (Bürgmann, 1993).

1. Postseismic relaxation below Loma Prieta rupture

We constrain models of postseismic slip below the rupture to be of the same strike and dip as the earthquake rupture and to lie at 18 km (center of model fault). If we loosen the depth constraint, the inversion always favors the shallowest possible model fault. A reduced $\chi^2$-value of 8.46 (Table 2) indicates that models of postseismic relaxation below the earthquake rupture fit the data very poorly. In particular the deep source fails to reproduce the fault-normal displacements along the Loma Prieta profile. The fit to the leveling data, however, is comparable to models involving shallower sources.

2. Slip and/or contraction on Loma Prieta rupture zone

If we remove the depth constraint on slip along the Loma Prieta rupture, the fit improves significantly. The model fault lies close to the Loma Prieta rupture, but favors a very large fault width of 20 km (upper bound of permitted range) with 3 and 6 cm/yr of thrusting and strike-slip, respectively. However, a reduced $\chi^2$-value of 7.46 indicates that the model is not able to adequately fit the data.

Savage and others (1994) suggest that fault-zone compaction following the Loma Prieta rupture may explain the fault-normal motion. We find that the addition of opening motion to the list of fault parameters improves the model fit significantly (reduced $\chi^2$-value of 4.62). The inversion favors a fault of maximum permitted width (20 km) with 4 cm/yr of thrusting, 5 cm/yr of strike-slip, and 3 cm/yr of fault-zone compaction.

3. Models of slip and/or collapse on Loma Prieta rupture zone and slip below

We examine the displacements from slip and compaction along the Loma Prieta rupture together with accelerated fault creep below. This represents a combination of the previous models. We find that adding a second fault below the Loma Prieta rupture does not improve the model fit. The GPS and leveling data do not reveal any deep accelerated deformation below the Loma Prieta rupture.

4. Models including reverse fault slip NE of San Andreas fault

We find that a model that includes slip on two faults, reverse and strike-slip on a vertical fault in the San Andreas fault zone and thrusting on a southwest dipping fault northeast of the San Andreas, provides the best fit to the data. The faults are not allowed to dip to the northeast or to undergo normal slip to avoid geologically unreasonable geometries, and strike-slip is always right-lateral.

| Data | Model | | Length along strike (km) | Depth to center (km) | Width along dip (km) | Dip (° SW) | Azimuth (°) | Location East (km) | Location North (km) | Dip-slip (m/yr) | Strike-slip (m/yr) | Opening (m/yr) | Chisq (GPS) | Chisq | reduced Chisq |
|---|---|---|---|---|---|---|---|---|---|---|---|---|---|---|---|
| GPS & | Down-dip of LP fault | | 32.48 | ***18*** | 1.43 | ***70*** | ***132*** | -3.44 | -0.96 | -0.29 | 1.90 | *none* | 688.5 | 794.9 | 8.46 |
| leveling | fault slip only | | | | | | | | | | | | | | |
| GPS & | "Loma Prieta fault" | | 33.54 | 13.88 | 20* | ***70*** | ***132*** | -3.03 | 3.74 | -0.03 | 0.06 | *none* | 540.3 | 663.7 | 7.46 |
| leveling | fault slip only | | | | | | | | | | | | | | |
| GPS & | "Loma Prieta fault" | | 37.42 | 14.16 | 20* | ***70*** | ***132*** | -1.49 | 2.25 | -0.04 | 0.05 | -0.03 | 313.1 | 411.0 | 4.62 |
| leveling | with fault zone collapse | | | | | | | | | | | | | | |
| GPS & | LP fault slip & collapse | A | 37.62 | 9.1 | 7.64 | ***70*** | ***132*** | -0.86 | 4.82 | -0.06 | 0.05 | -0.04 | 298.1 | 392.9 | 4.73 |
| leveling | and creep below | B | 20.78 | ***18*** | ***5*** | ***70*** | ***132*** | -2* | -2* | -0.09 | 0.33 | *none* | | | |
| GPS & | 2-fault model | A | 59.87 | 7.93 | 7.76 | -89.96 | 138.91 | 7.71 | -1.42 | -0.06 | 0.05 | *none* | 182.9 | 264.8 | 3.40 |
| leveling | SAF and thrust | B | 45* | 4.52 | 8.26 | -34.71 | 138.8 | 1* | 6.85 | -0.06 | 0* | *none* | | | |
| *GPS &* | *2-fault model* | *A* | *45.00* | *7* | *11* | *-89* | *138* | *6.10* | *0.33* | *-0.02* | *0.02* | *none* | | | *2.20* |
| *leveling* | *(1990 - 1994)* | *B* | *41.00* | *4* | *8.5* | *-43* | *135* | *1.80* | *9.90* | *0.03* | *0** | *none* | | | |

* Hit upper or lower boundary of parameter range

Table 2. Model fault parameters from non-linear inversion of postseismic GPS and leveling data. The first five models are derived from GPS data collected between 1989 to 1993. The sixth model considers displacements between April 1990 and April 1994.

A reduced $\chi^2$-value of 3.4 indicates that the model does not fully explain the data within the reported errors. This may be caused by an underestimate of the errors in the GPS pre- to postseismic comparison and the leveling data. Alternatively the misfit may indicate that our model insufficiently represents the physical processes responsible for the deformation. Material heterogeneities, multiple fault surfaces, complex slip distributions, distributed inelastic deformation may contribute to the misfit.

Adding the additional constraints from stations of the Santa Cruz Mountains network improved our resolution of the width of the aseismic slip patch. Figure 8a shows the surface projection of the best-fitting two model faults. Overall the model is quite similar to the previously determined model (Table 2) and confirms the two aseismically slipping faults. Figure 8b shows the observed and predicted elevation changes along the leveling line from the best two fault model. The model does not predict the continued subsidence pattern at the NE end of the leveling line and overpredicts uplift of the area near Loma Prieta (Figure 6).

*Discussion of model results*

Our model involves contemporaneous oblique-slip and thrust faulting at high rates on two faults with similar strikes. The inferred slip on the San Andreas fault from about 4 to 10 km depth may represent creep above the two high-slip asperities that released most of the earthquake moment (Beroza, 1991; Hartzell et al., 1991; Wald et al., 1991). The reverse component on the vertical fault may be caused by the stress perturbation from the obliquely slipping Loma Prieta rupture. Note that the average displacement rates, and model slip rates are smaller in the 1990 to 1994 comparison than in the previous models. We find clear evidence that deformation rates decayed within about 3 years following the event, however, more observations are needed to fully contrain the time constants involved in the postseismic transients.

How unique is our model of aseismic creep along the Foothills thrust belt together with aseismic slip along the SAF above the coseismic rupture, following the 1989 Loma Prieta earthquake? Even though surface deformation data can not, on their own, uniquely constrain the kinematics of the deformation source, we feel confident that our model is the best first-order representation of postseismic defornation following the earthquake. The 2-fault model is the simplest model that adequately fits the data (Table 2). In reality, the observed strain field is probably produced by more complex fault geometries, but the overall pattern is well predicted by the model. We do not find that a model involving fault zone collapse satisfactorily fits the data (Table 2). The model makes sense in the neotectonic context of the area (Bürgmann et al., 1994). Geologic, geomorphic and geodetic data all suggest that the Foothills thrust belt must be an active deformation zone that produces about 1 mm/yr of uplift of the southern Santa Cruz Mountains. Our data suggest that some of this uplift occurred since the 1989 earthquake. Finally, the model makes sense as a possible response to the static stress field of Loma Prieta earthquake that increased shear stress on thrust faults in the region where we observe anomalous contraction (see discussion below). We do not yet see evidence for deep shear of flow below the rupture zone, a feature inherent in most models of postseismic deformation.

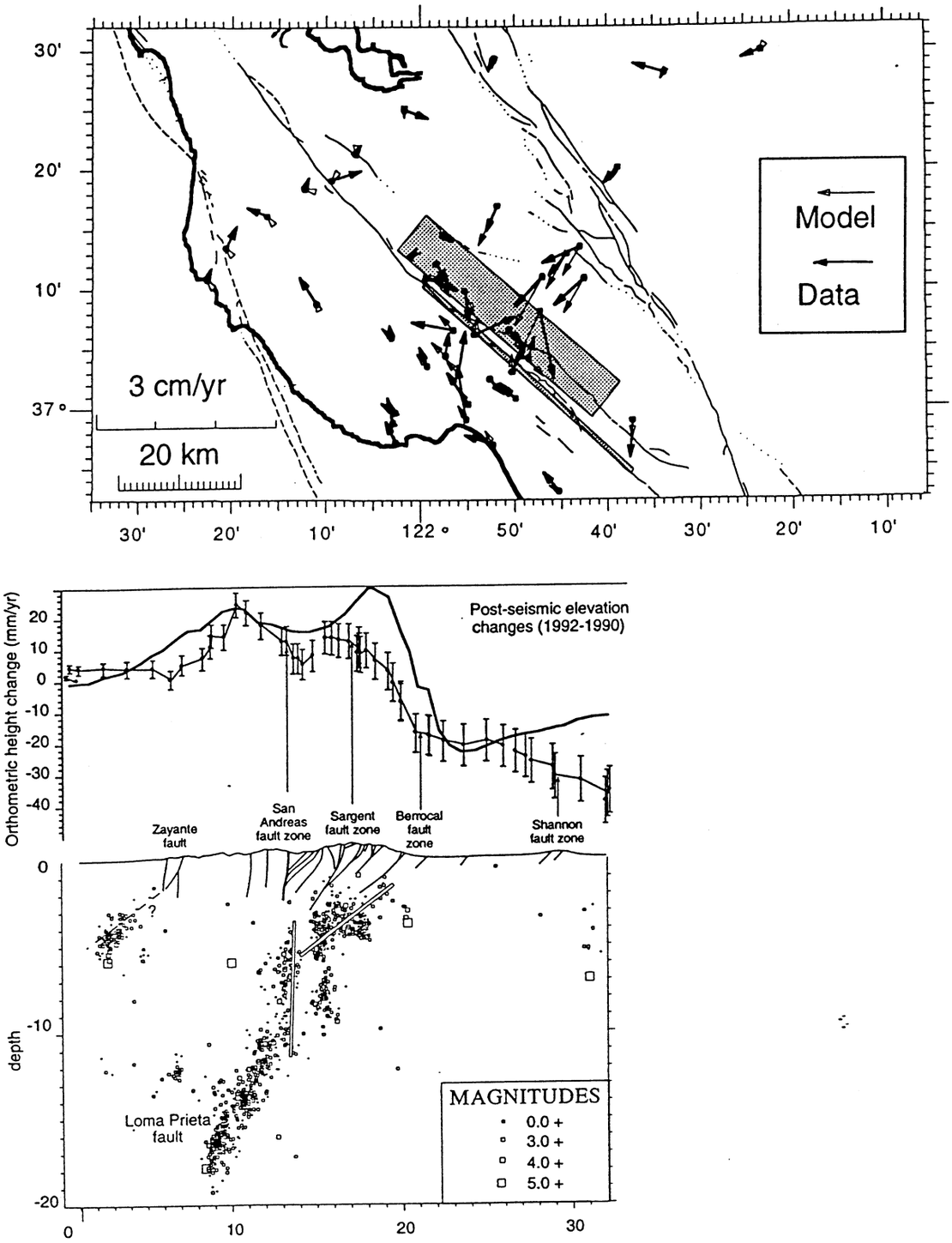


**Figure 8.** (a) Postseismic station velocities with preseismic displacement rates subtracted from measured rates. Also shown are the displacements computed from a boundary element model involving slip on two faults. The two rectangles show the projections of the faults used to compute the modeled station displacements. (b) Cross-section showing the two model faults and aftershocks. The first fault lies approximately in the vertical band of San Andreas fault seismicity above the Loma Prieta rupture, the second fault lies in a cluster of seismicity NE of the San Andreas fault.

# DISCUSSION

*Thrusting northeast of the San Andreas Fault*

Northeast of the San Andreas fault are several sub-parallel SW-dipping faults, including the Monte Vista, Berrocal, and Shannon faults (Figure 13, (Aydin and Page, 1984)), with a dominant component of thrust motion (McLaughlin, 1990). Some of these faults appear to have been active in the Quaternary as evidenced by offset young alluvial deposits and soil horizons (Haugerud and Ellen, 1990; McLaughlin, 1990). Broad zones of compressional surface deformation during the Loma Prieta earthquake follow the trend of these fault zones intermittently over a total distance of ~20 km (Haugerud and Ellen, 1990). Our model thrust fault appears to coincide with the Berrocal fault zone, but it is possible that postseismic slip is distributed between several faults of the complex Foothills thrust system of the Santa Cruz Mountains.

The modeled reverse fault lies close to the Berrocal fault zone and has a comparable dip (McLaughlin, 1990). This zone has experienced strongly increased earthquake activity since the Loma Prieta event (Reasenberg and Simpson, 1992). Focal mechanisms of all post-Loma Prieta earthquakes > M 2.0 near the Berrocal fault zone, NE of the San Andreas, indicate that these events occurred predominantly on reverse faults (Bürgmann et al., 1995). The seismicity near the Loma Prieta rupture on the other hand is very complex with all types of fault plane solutions (Oppenheimer, 1990). Note that the fault slip we model exceeds by several orders of magnitude the slip accumulated in aftershocks and must be aseismic.

Stress redistribution accompanying the Loma Prieta mainshock would increase the loading on thrust faults NE and updip of the rupture (Reasenberg and Simpson, 1992). Figure 9 shows a cross-section perpendicular to the San Andreas fault with the contoured coseismic stress changes on thrust faults NE of the San Andreas overlaid on a plot of the aftershocks. Shear stress changes and the thrust-normal stress changes both affect the loading of N60°W striking, 45° dipping thrust planes through a Coulomb Failure Function (Reasenberg and Simpson, 1992)

$$CFF = \tau_s + \mu\sigma_n,$$

where $\tau_s$ is the shear traction in the dip direction, $\sigma_n$ the fault-normal traction, and $\mu$ the coefficient of friction. A coefficient of friction of 0.6 has been chosen for the model in Figure 18. As the complex slip distribution during the earthquake is expected to be important in the induced stress field in the close vicinity of the earthquake rupture we used the heterogeneous fault slip model of Beroza (1991) to compute the stress changes. Co-seismically induced stress changes of 1 to 2 MPa that enhance thrust loading occurred NE of the San Andreas fault. The stress changes on fault planes of somewhat different strikes and dips are comparable to those shown. Apparently the increased micro-seismicity and the aseismic thrusting inferred from geodetic data reflect deformation in response to the load increase. The induced seismicity near the Berrocal fault zone is restricted to a ~ 15 km wide zone along the northern half of the Loma Prieta rupture (Figure 17). This may be related to the observation that most of the thrust component of the earthquake slip is concentrated NW of the Loma Prieta epicenter (Beroza, 1991; Hartzell et al., 1991; Wald et al., 1991).

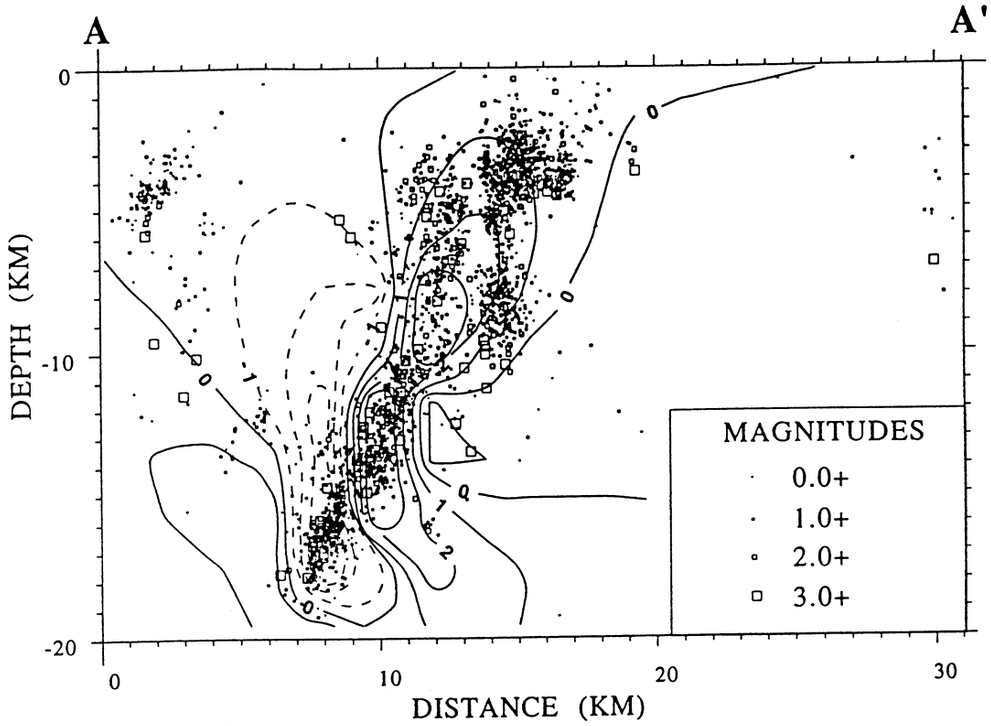


Figure 10 Contoured stress changes (in MPa) induced by the Loma Prieta earthquake on 45° SW dipping fault planes. The coseismic displacement distribution determined by Beroza (1991) is discretized into 272 uniform slip fault elements in an elastic, isotropic, and homogeneous halfspace. Both fault-normal stresses and dip-parallel shear stresses influence the faults through a Coulomb failure criterion with a coefficient of friction $\mu = 0.6$.

An enigma associated with the Loma Prieta earthquake was the observation that the highest topography of the Santa Cruz Mountains around Loma Prieta subsided by ~10 cm during the earthquake (Lisowski et al., 1990a). Long term uplift rates in the Loma Prieta area deduced from apatite fission track dating and geomorphic analyses average about 1 mm/yr over the last 5 Ma (Bürgmann et al., 1994). This agrees with uplift-rate estimates of McLaughlin in the Sierra Azul block NE of the San Andreas based on structural and stratigraphic evidence. While different fault-plane geometries could produce the long-term uplift pattern (Schwartz et al., 1990), slip on the reverse faults at the base of the southern Santa Cruz Mountains at combined rates of 2-3 mm/yr would result in the topographic expression of the southern Santa Cruz Mountains (Arrowsmith et al., 1992). Our measurements indicate that some of this uplift may occur concurrently with aseismic fault slip at depth on the Berrocal fault zone.

*Postseismic rate changes*

Models based on only the first two years of GPS data suggested more than twice the fault slip rates of our current model (Bürgmann et al., 1992). An inspection of the fault-normal and fault-parallel displacement components suggests that there may be a consistent decrease of the postseismic rates (Savage et al., 1994). Future work is planned to develop a model of the postseismic deformation that includes a possible rate change in the analysis. Additional GPS surveys are needed to constrain the time constants of the decaying strain signal.

# IMPLICATIONS FOR SEISMIC HAZARD IN THE SAN FRANCISCO BAY REGION

Continued slip at decimeter rates on faults in the San Francisco Bay region will change the loading of nearby segments of the San Andreas fault and the Hayward fault. We modeled the change in loading on NW striking fault planes due to the Loma Prieta earthquake and postseismic fault slip with the method outlined above, assuming that fault-parallel shear stress as well as fault normal stresses determine the fault response through a Coulomb failure criterion. A detailed analysis of coseismic static stress changes on Bay area faults shows that micro-seismicity rates increased, or decreased, in accordance with the computed stresses (Reasenberg and Simpson, 1992). Reduced creep rates, observed along the southern Hayward fault following the earthquake, are evidence of induced left-lateral shear stress across that segment of the fault (Lienkaemper et al., 1992).

We computed the contoured changes in frictional failure conditions for right lateral strike-slip shear on NW striking fault planes at a depth of 10 km due to the coseismic rupture and from the predicted postseismic fault slip in the year following the earthquake (Bürgmann et al., 1995). We find that the postseismic fault slip further increases the load on the San Andreas fault immediately to the NW of the Loma Prieta rupture, while the combined coseismic and postseismic effects have a retarding effect on the Hayward fault zone and most of the Calaveras and San Gregorio-Hosgri fault zones. The yearly postseismic stress changes are about an order of magnitude less than those induced coseismically. If the Loma Prieta earthquake stress changes advanced the occurrence of the next earthquake N of the rupture by 2-25 years (Reasenberg and Simpson, 1992), then the postseismic changes enhance this effect by almost 10% per year.

Similar postseismic adjustments occurred following the 1979 Coyote Lake and the 1984 Morgan Hill earthquakes along the Calaveras fault (Oppenheimer et al., 1990). While the coseismic stress perturbations on neighboring fault segments induced by these moderate earthquakes were negligible (Du and Aydin, 1993), postseismic fault creep adjacent to the coseismic ruptures may have caused the observed south-to-north propagation of earthquakes along the Calaveras fault (Oppenheimer et al., 1990).

The stress changes caused by co- and postseismic fault slip only add to those accumulated by background loading of the Bay area faults. If a fault is near its breaking point the stress release associated with the Loma Prieta earthquake may only slightly retard the imminent failure. The January 15, 1993 Gilroy earthquake that occurred in a region of induced left-lateral shear, east of the southern termination of the Loma Prieta rupture is a timely reminder of this. The peninsular segment of the San Andreas fault, the updip extension of the Loma Prieta rupture (from about 8 km to the surface), and several thrust faults that parallel the San Andreas through most of the Bay region, appear to represent significant seismic hazards since the Loma Prieta earthquake. Continued reverse faulting may also relieve normal traction along the southern Hayward fault and increase the likelihood of faulting there, despite a decrease in right-lateral stress.

Rapid fault slip on the Berrocal fault zone since the Loma Prieta earthquake could be a precursory phenomenon to a future earthquake on this fault. While records of historic seismicity in the area reach only as far back as the early 19th century, they show that the last 80 years have been marked by unusual seismic quiescence. In 1865, a ~M 6.5 earthquake may have ruptured a thrust

fault NE of the San Andreas with two > M 5 foreshocks in the preceding year (Tuttle and Sykes, 1992). This earthquake was preceded by a M ~ 7 break in 1838 that involved the peninsular San Andreas fault segment and maybe the Loma Prieta fault segment, and followed in 1868 by a large earthquake on the southern Hayward fault (e.g., (Tuttle and Sykes, 1992). An earthquake comparable to the 1865 event constitutes a significant hazard to the south San Francisco Bay region. Our results suggest one possible mechanism by which earthquakes may influence the seismicity in the region in the years following the original rupture.

## REFERENCES


Anderson, D. L., 1975, Accelerated plate tectonics: Science, v. 187, p. 1077-1079.

Arnadottir, T., and Segall, P., 1994, The 1989 Loma Prieta earthquake imaged from inversion of geodetic data: J. Geophys. Res., v. 99, p. 21,835-.

Arrowsmith, R., Bürgmann, R., and Dumitru, T., 1992, Uplift of the southern Santa Cruz Mountains deduced from fission-track dating and geomorphic analyses: EOS Trans. AGU, v. 73, p. in press.

Aydin, A., and Page, B. M., 1984, Diverse Pliocene-Quaternary tectonics in a transform environment, San Francisco Bay region, California: Geol. Soc. Am. Bull., v. 95, p. 1303-1317.

Behr, J., Bilham, R., and Bodin, P., 1993, Increased surface creep rates on the San Andreas fault southeast of the Loma Prieta mainshock: U.S. Geol. Surv. Prof. Pap., v. 1550, p. in review.

Behr, J., Bilham, R., Bodin, P., Burford, R. O., and Bürgmann, R., 1990, Aseismic slip on the San Andreas fault south of Loma Prieta: Geophys. Res. Lett., v. 17, no. 9, p. 1445-1448.

Beroza, G. C., 1991, Near-source modeling of the Loma Prieta earthquake: Evidence for heterogeneous slip and implications for earthquake hazard: Bull. Seism. Soc. Am., v. 81, p. 1603-1621.

Beutler, G., Bauersima, I., Gurtner, W., Rothacher, M., Schildknecht, T., Mader, G. L., and Abell, M. D., 1987, Evaluation of the 1984 Alaska Global Positioning System campaign with the Bernese GPS software: J. Geophys. Res., v. 92, p. 1295-1303.

Bilham, R., 1989, Surface slip subsequent to the 24 November 1987 Superstition Hills, California, earthquake monitored by digital creepmeters: Bull. Seism. Soc. Am., v. 79, p. 424-450.

Bott, N. H. P., and Dean, D. S., 1973, Stress diffusion from plate boundaries: Nature, v. 243, p. 339-341.

Budianski, B., and Amazigo, C., 1976, Interaction of fault slip and lithosphere creep: J. Geophys. Res., v. 81, p. 4897-4900.

Bürgmann, R., 1993, Deformation associated with strike-slip faults [PhD thesis, 186 pp. thesis]: Stanford University, Stanford, CA.

Bürgmann, R., Arrowsmith, R., Dumitru, T. A., and McLaughlin, R. J., 1994, Rise and fall of the southern Santa Cruz Mountains, California, from fission tracks, geomorphology, and geodesy: J. Geophys. Res., v. 99, no. B10, p. 20,181-20,202.

Bürgmann, R., and Segall, P., 1991, Postseismic GPS monitoring NW of the 1989 Loma Prieta rupture zone: EOS Trans. AGU, v. 72, no. 44, p. 119.

Bürgmann, R., Segall, P., Lisowski, M., Marshall, G., Stein, R., and Svarc, J. P., 1993, Post-seismic uplift of the southern Santa Cruz Mountains following the Loma Prieta earthquake: EOS Trans. AGU, v. 74, no. 16, p. 106.

Bürgmann, R., Segall, P., Lisowski, M., and Svarc, J. P., 1992, Rapid aseismic slip on the Berrocal fault zone following the Loma Prieta earthquake: EOS Trans. AGU, v. 73, no. 43, p. 119.

Bürgmann, R., Segall, P., Lisowski, M., and Svarc, J. P., 1995, Post-seismic strain following the 1989 Loma Prieta earthquake from repeated GPS measurements: U.S. Geol. Surv. Prof. Pap., v. 1550, p. in press.

Clark, T. A., Ma, C., Sauber, J. M., Ryan, J. W., Gordon, D., Shaffer, D. B., Caprette, D. S., and Vandenberg, N. R., 1990, Geodetic measurements of deformation in the Loma Prieta, California earthquake with Very Long Baseline Interferometry: Geophys. Res. Lett., v. 17, no. 8, p. 1215-1218.

Cohen, S. C., 1979, Postseismic surface deformations due to lithospheric and asthenospheric viscoelasticity: Geophys. Res. Lett., v. 6, no. 3, p. 129-131.

Davis, J. L., Prescott, W. H., Svarc, J. L., and Wendt, K. J., 1989, Assesment of Global Positioning System measurements for studies of crustal deformation: J. Geophys. Res., v. 94, p. 13635-13650.

Dietz, L. D., and Ellsworth, W. L., 1990, The October 17, 1989, Loma Prieta, California, earthquake and its aftershocks: Geometry of the sequence from high-resolution locations: Geophys. Res. Lett., v. 17, p. 1417-1420.

Dixon, T. H., 1991, An introduction to the global positioning system and some geological applications: Reviews of Geophysics, v. 29, p. 249-276.

Du, Y., and Aydin, A., 1993, Stress transfer during three sequential moderate earthquakes along the

central Calaveras fault, California: J. Geophys. Res., v. 98, p. 9947-9962.

Du, Y., Aydin, A., and Segall, P., 1992, Comparison of various inversion techniques as applied to the determination of a geophysical deformation model for the 1983 Borah Peak earthquake: Bull. Seism. Soc. Am., v. 82, p. 1840-1866.

Ellsworth, W. L., 1990, Earthquake history, 1769-1989, *in* Wallace, R. E., ed., The San Andreas fault system, Calfornia, U.S. Geological Survey Professional Paper, p. 153-181.

Gwyther, R. L., Gladwin, M. T., and Hart, R. H. G., 1992, A shear strain anomaly following the Loma Prieta earthquake: Nature, v. 356, no. 6365, p. 142-144.

Hager, B. H., King, R. W., and Murray, M. H., 1991, Measurements of crustal deformation using the Global Positioning System: Annu. Rev. Earth Planet. Sci., v. 19, p. 351-382.

Hartzell, S. H., Stewart, G. S., and Mendoza, C., 1991, Comparison of $L_1$ and $L_2$ norms in a teleseismic waveform inversion for the slip history of the Loma Prieta, California, earthquake: Bull. Seism. Soc. Am. Bull., v. 81, no. 5, p. 1518-1539.

Haugerud, R. A., and Ellen, S. D., 1990, Coseismic ground deformation along the northeast margin of the Santa Cruz Mountains, *in* Schwartz, D. P., and Ponti, D. J., eds., Field guide to neotectonics of the San Andreas fault system, Santa Cruz Mountains, in light of the Loma Prieta earthquake, U.S. Geological Survey, Open File Report, p. 32-37.

Kasahara, K., 1981, Earthquake mechanics, Cambridge Earth Science Series: Cambridge, Cambridge University Press, 248 p.

King, G. C. P., Lindh, A. G., and Oppenheimer, D. H., 1990, Seismic slip, segmentation, and the Loma Prieta earthquake: Geophys. Res. Lett., v. 17, no. 9, p. 1449-1452.

Kovach, R. L., and Beroza, G. C., 1993, Seismic potential from reverse faulting on the San Francisco Peninsula: Bull. Seism. Soc. Am., v. 83, no. 2, p. 597-602.

Langbein, J. O., 1990, Post-seismic slip on the San Andreas fault at the northwestern end of the 1989 Loma Prieta earthquake rupture zone: Geophys. Res. Lett., v. 17, p. 1223-1226.

Larson, K. M., and Agnew, D. C., 1991, Application of the Global Postioning System to crustal deformation measurements 1. Precision and accuracy: J. Geophys. Res., v. 96, p. 16547-16565.

Larson, K. M., Webb, F. H., and Agnew, D. C., 1991, Application of the Global Postioning System to crustal deformation measurements 2. The influence of errors in orbit determination networks: J. Geophys. Res., v. 96, p. 16567-16584.

Lawson, J. J., 1908, The California earthquake of April 18, 1906: Report of the State Earthquake Investigation Commission, Carnegie Institution of Washington Publication.

Lehner, F. K., Li, V. C., and Rice, J. R., 1981, Stress diffusion along rupturing plate boundaries: J. Geophys. Res., v. 86, p. 6155-6169.

Li, V. C., and Rice, J. R., 1987, Crustal deformation in great California earthquake cycles: J.Geophys.Res., v. 92, p. 11533-11551.

Lienkaemper, J. J., Galehouse, J. S., and Simpson, R. W., 1992, Hayward fault, California: Longterm creep rates versus slower creep since 1989 Loma Prieta earthquake: EOS Trans. AGU, v. 73, p. 119.

Linker, M. F., and Rice, J. R., 1991, The effective viscosity of the San Andreas fault beneath the seismogenic zone: Constraints from the response to the 1989 Loma Prieta earthquake: EOS Trans. AGU, v. 72, no. 44, p. 310-311.

Linker, M. F., and Rice, J. R., 1995, Models of postseismic deformation and stress transfer associated with the 1989 Loma Prieta earthquake: U.S. Geol. Surv. Prof. Pap., v. 1550, p. in press.

Lisowski, M., Prescott, W. H., Savage, J. C., and Johnston, M. J., 1990a, Geodetic estimate of coseismic slip during the 1989 Loma Prieta, California earthquake: Geophys. Res. Lett., v. 17, no. 9, p. 1437-1440.

Lisowski, M., Prescott, W. H., Savage, J. C., and Svarc, J. L., 1990b, A possible geodetic anomaly observed prior to the Loma Prieta, California, earthquake: Geophys. Res. Lett., v. 17, no. 8, p. 1211-1214.

Lisowski, M., Savage, J. C., and Prescott, W. H., 1991a, Surface deformation after the Loma Prieta, California, earthquake: EOS Trans. AGU, v. 72, no. 44, p. 119.

Lisowski, M., Savage, J. C., and Prescott, W. H., 1991b, The velocity field along the San Andreas fault in central and southern California: J. Geophys. Res., v. 96, no. B5, p. 8369-8389.

Marshall, G. A., Stein, R. S., and Thatcher, W., 1991, Faulting geometry and slip from co-seismic elevation changes: The October 17, 1989 Loma Prieta, California, earthquake: Bull. Seism. Soc. Am., v. 81, p. 1660-1693.

Matsu'ura, M., Jackson, D. D., and Cheng, A., 1986, Dislocation model for aseismic crustal deformation at Hollister, California: J. Geophys. Res., v. 91, p. 12661-12674.

McLaughlin, R., 1990, Stop 4. Sargent fault zone at Loma Prieta, *in* Schwartz, D. D., and Ponti, D. J., eds., Field guide to neotectonics of the San Andreas fault system, Santa Cruz Mountains, in light of the 1989 Loma Prieta earthquake: Menlo

Park, U.S. Geological Survey Open File Report, p. 19-22.
Nur, A., and Mavko, G., 1974, Postseismic viscoelastic rebound: Science, v. 183, p. 204-206.
Okada, Y., 1985, Surface deformation due to shear and tensile faults in a half-space: Bull. Seism. Soc. Am., v. 75, p. 1135-1154.
Oppenheimer, D. H., 1990, Aftershock slip behavior of the 1989 Loma Prieta, California earthquake: Geophys. Res. Lett., v. 17, no. 8, p. 1199-1202.
Oppenheimer, D. H., Bakun, W. H., and Lindh, A. G., 1990, Slip partitioning of the Calaveras fault, California, and prospects for future earthquakes: J. Geophys. Res., v. 95, no. B6, p. 8483-8498.
Reasenberg, P. A., and Simpson, R. W., 1992, Response of regional seismicity to the static stress change produced by the Loma Prieta earthquake: Science, v. 255, p. 1687-1690.
Rothacher, M., Beutler, G., Gurtner, W., Schildknecht, T., and Wild, U., 1990, Documentation for Bernese GPS Software Version 3.2: Bern, University of Bern.
Rundle, J. B., and Jackson, D. D., 1977, A three-dimensional viscoelastic model of a strike-slip fault: Geophys. J. R. Astron. Soc., v. 49, p. 575-591.
Rymer, M. J., 1990, Near-fault measurement of postseismic slip associated with the 1989 Loma Prieta, California, earthquake: Geophys. Res. Lett., v. 17, no. 10, p. 1789-1792.
Savage, J. C., 1971, A theory of creep waves propagating along a transform fault: J. Geophys. Res., v. 76, p. 1954-1966.
Savage, J. C., Lisowski, M., and Svarc, J. L., 1994, Postseismic deformation following the 1989 (M = 7.1) Loma Prieta, California, earthquake: J. Geophys. Res., v. 99, p. 13757-13765.
Savage, J. C., and Prescott, W. H., 1978, Asthenosphere readjustment and the earthquake cycle: J. Geophys. Res., v. 83, p. 3369-3376.
Scholz, C. H., 1977, A physical interpretation of the Haicheng earthquake prediction: Nature, v. 267, no. 5607, p. 121-124.
Schwartz, S. Y., Orange, D. L., and Anderson, R. S., 1990, Complex fault interactions in a restraining bend on the San Andreas fault, southern Santa Cruz Mountains, California: Geophys. Res. Lett., v. 17, no. 8, p. 1207-1210.
Smith, S. W., and Wyss, M., 1968, Displacement on the San Andreas fault subsequent to the 1966 Parkfield earthquake: Bull. Seism. Soc. Am., v. 58, p. 1955-1973.
Snay, R. A., Neugebauer, H. C., and Prescott, W. H., 1991, Horizontal deformation associated with the Loma Prieta earthquake: Bull. Seism. Soc. Am., v. 81, p. 1647-1659.
Steidl, J. H., Archuleta, R. J., and Hartzell, S. H., 1991, Rupture history of the 1989 Loma Prieta, California, earthquake: Bull. Seism. Soc. Am., v. 81, p. 1573-1602.
Thatcher, W., 1974, Strain release mechanism of the 1906 San Francisco earthquake: Science, v. 184, p. 1283-1285.
Thatcher, W., 1983, Nonlinear strain buildup and the earthquake cycle on the San Andreas fault: J. Geophys. Res., v. 88, p. 5893-5902.
Thatcher, W., 1986, Cyclic deformation related to great earthquakes at plate boundaries, Recent Crustal Movements of the Pacific Region: Wellington, New Zealand, Royal Society of New Zealand Bulletin, p. 245-272.
Toksöz, M. N., Shakal, A. F., and Michael, A. J., 1979, Space-time migration of earthquakes along the North Anatolian fault zone and seismic gaps: Pageoph, v. 117, p. 1258-1270.
Tuttle, M. P., and Sykes, L. R., 1992, Re-evaluation of several large historic earthquakes in the vicinity of the Loma Prieta and Peninsular segments of the San Andreas fault, California: Bull. Seism. Soc. Am., v. 82, no. 4, p. 1802-1820.
Wald, D. J., Helmberger, D. V., and Heaton, T. H., 1991, Rupture model of the 1989 Loma Prieta earthquake from the inversion of strong-motion and broadband teleseismic data: Bull. Seism. Soc. Am., v. 81, no. 5, p. 1540-1572.
Williams, C. R., Arnadottir, T., and Segall, P., 1993, Coseismic deformation and dislocation models of the 1989 Loma Prieta earthquake derived from Global Positioning System measurements: J. Geophys. Res., v. 98, p. 4567-4578.
Wood, M. D., and Allen, S. S., 1973, Recurrence of seismic migrations along the central California segment of the San Andreas fault system: Nature, v. 244, p. 213-215.

Bibliography of publications related to this work:


Bürgmann, R., Arrowsmith, R., and Dumitru, T., 1994, Slip Rates and Earthquake Hazard Along the Foothills Thrust Belt in the Southern San Francisco Bay Area, *USGS Open File Report, p. 31-33.*

Bürgmann, R., Segall, P., Arrowsmith, R., and Dumitru, T., 1994, Slip rates and earthquake hazard along the Foothills thrust belt in the Southern Santa Cruz Mountains, *GSA Abstracts with Program*, v. 26, no. 7, p. 191.

Bürgmann, R., Segall, P., Lisowski, M., and Svarc, J.L., 1994, Five years of post-seismic strain following the Loma Prieta earthquake, *EOS Trans. AGU*, v.75,.p. 177.

Bürgmann, R., Segall, P., Lisowski, M., and Svarc, J.L., 1994, Strain development subsequent to the 1989 Loma Prieta earthquake, *U.S.G.S. Professional Paper 1550D, in press.*

Bürgmann, R., Segall, P., Lisowski, M., and Svarc, J.L., 1995, Decay of postseismic strain anomaly following the 1989 Loma Prieta, California, earthquake, subm. to IUGG 1995.